

A tale of two morphs: developmental patterns and mechanisms of seed coat differentiation in the dimorphic diaspore model *Aethionema arabicum* (Brassicaceae)

Waheed Arshad¹ , Teresa Lenser², Per K. I. Wilhelmsson³ , Jake O. Chandler¹ , Tina Steinbrecher¹ , Federica Marone⁴ , Marta Pérez¹ , Margaret E. Collinson⁵, Wolfgang Stuppy^{6,7}, Stefan A. Rensing³ , Günter Theißen²  and Gerhard Leubner-Metzger^{1,8,*} 

¹Department of Biological Sciences, Royal Holloway University of London, Egham TW20 0EX, UK,

²Matthias Schleiden Institute/Genetics, Friedrich Schiller University Jena, Jena D-07743, Germany,

³Plant Cell Biology, Department of Biology, University of Marburg, Marburg D-35043, Germany,

⁴Swiss Light Source, Paul Scherrer Institute, Villigen CH-5232, Switzerland,

⁵Department of Earth Sciences, Royal Holloway University of London, Egham TW20 0EX, UK,

⁶Botanischer Garten der Ruhr-Universität Bochum, Universitätsstraße 150, Bochum D-44780, Germany,

⁷The Royal Botanic Gardens, Kew, Wellcome Trust Millennium Building, Wakehurst Place, Ardingly, West Sussex RH17 6TN, UK, and

⁸Laboratory of Growth Regulators, Palacký University, Institute of Experimental Botany, Czech Academy of Sciences, Olomouc CZ-78371, Czech Republic

Received 5 March 2021; accepted 15 April 2021; published online 4 May 2021.

*For correspondence (e-mail gerhard.leubner@rhul.ac.uk).

SUMMARY

The developmental transition from a fertilized ovule to a dispersed diaspore (seed or fruit) involves complex differentiation processes of the ovule's integuments leading to the diversity in mature seed coat structures in angiosperms. In this study, comparative imaging and transcriptome analysis were combined to investigate the morph-specific developmental differences during outer seed coat differentiation and mucilage production in *Aethionema arabicum*, the Brassicaceae model for diaspore dimorphism. One of the intriguing adaptations of this species is the production and dispersal of morphologically distinct, mucilaginous and non-mucilaginous diaspores from the same plant (dimorphism). The dehiscent fruit morph programme producing multiple mucilaginous seed diaspores was used as the default trait combination, similar to *Arabidopsis thaliana*, and was compared with the indehiscent fruit morph programme leading to non-mucilaginous diaspores. Synchrotron-based radiation X-ray tomographic microscopy revealed a co-ordinated framework of morph-specific early changes in internal anatomy of developing *A. arabicum* gynoecia including seed abortion in the indehiscent programme and mucilage production by the mucilaginous seed coat. The associated comparative analysis of the gene expression patterns revealed that the unique seed coat dimorphism of *Ae. arabicum* provides an excellent model system for comparative study of the control of epidermal cell differentiation and mucilage biosynthesis by the mucilage transcription factor cascade and their downstream cell wall and mucilage remodelling genes. Elucidating the underlying molecular framework of the dimorphic diaspore syndrome is key to understanding differential regulation of bet-hedging survival strategies in challenging environments, timely in the face of global climatic change.

Keywords: *Aethionema arabicum*, bet-hedging, developmental anatomy, diaspore dimorphism, fruit development, phenotypic plasticity, reproductive development, seed coat mucilage, synchrotron radiation X-ray tomographic microscopy, transcription factors.

INTRODUCTION

Fruit and seed development represent a crucial phase of angiosperm reproduction. The transition from the flower

after pollination into the diversity of mature dispersal units, i.e., fruits and seeds (diaspores), is particularly important for annual plant species whose life-cycle is entirely dependent on successful diaspore production,

dispersal and regeneration from seed (Baskin and Baskin, 2014; Finch-Savage and Leubner-Metzger, 2006; Linkies *et al.*, 2010; Roeder and Yanofsky, 2006; Walck *et al.*, 2011). Diaspore development in many plant model systems, including *Arabidopsis thaliana*, is monomorphic, i.e., only a single type (morph) of fruit and/or seed is produced. The default monomorphic 'bauplan' within the Brassicaceae is the development of dehiscent fruits (DEH) containing mucilaginous seeds (M^+) with *A. thaliana* and *Lepidium sativum* as examples (Ferrandiz *et al.*, 1999; Mühlhausen *et al.*, 2013; Scheler *et al.*, 2015). The DEH/ M^+ fruit/seed programme leads to fruit valve opening to release mature M^+ seeds as diaspores, which upon imbibition release mucilage from their outer seed coats (myxospermy) (Viudes *et al.*, 2020; Western, 2012; Yang *et al.*, 2012). Mutations in *A. thaliana* fruit development genes, such as the bHLH (basic helix-loop-helix) transcription factor (TF) *INDEHISCENT* and the MADS-box TFs *SHATTERPROOF1/2* (*SHP1/2*), block fruit valve opening which phenotypically result in indehiscent fruits (IND) (Mühlhausen *et al.*, 2013). In their phenotype, these mutants resemble species in which the IND fruits themselves serve as diaspores, i.e., the dispersal units are seeds encased by the fruit wall (pericarp). Fruit development in monomorphic species with IND fruits, such as *Lepidium appelianum*, is caused by reduced expression of these and other TFs of the dehiscence network.

Likewise, in many *A. thaliana* mutants, outer seed coat (testa) differentiation and mucilage production are impaired in TF genes such as *NAC-REGULATED SEED MORPHOLOGY1 and 2* [*NARS1/2*; plant-specific TFs of the NAC (NAM, ATAF and CUC) family], *GLABRA2* (*GL2*; a homeodomain TF), *MYB61*, *SHP1/2* and *SEEDSTICK* (*STK*; MADS-box TFs), or in downstream cell-wall remodelling protein (CWRP) genes (Golz *et al.*, 2018; Voiniciuc *et al.*, 2015; Western, 2012). Seeds of the *mucilage-modified* (*mum*) mutants fail either to release mucilage (*mum1*, *mum2*), to produce reduced quantities (*mum4*), or to have altered adherence of mucilage (*mum3*). Coupled with the development of either DEH or IND fruits is the development of seeds from fertilized ovules and the differentiation of the seed coat from the ovule integuments. In *A. thaliana* the two layers of the outer integument develop into the mucilage-accumulating testa and the three layers of the inner integument into the endothelium (Golz *et al.*, 2018; Voiniciuc *et al.*, 2015; Western, 2012). Upon imbibition of mature seeds, mucilage is extruded from the outer cell walls of mucilaginous cells in the testa. The testa epidermis and its mucilage secretory cells exhibit significant anatomical diversity also of taxonomic value within the Brassicaceae (Vaughan *et al.*, 1971). The main ecological adaptation of mucilaginous seed coats may be in facilitating imbibition and maintenance of moisture for growth in water-deficient environments, as well as in aiding or restricting diaspore dispersal (Arshad *et al.*,

2019; Baskin *et al.*, 2014; Gutterman, 2000; Western, 2012; Yang *et al.*, 2012).

Understanding how new morphologies, organs or body plans arise is one of the most fascinating questions in evolutionary developmental (evo-devo) plant biology. In contrast to monomorphic species, which produce only a single fruit and seed morph (monodiaspory), several angiosperm families independently evolved heteromorphism, characterized by the production of two or more distinct fruit and seed morphs (heterodiaspory) on individual plants (Baskin and Baskin, 2014; Baskin *et al.*, 2014; Imbert, 2002). The resultant heteromorphic diaspores differ in their morphological and physiological properties including size, shape, colour, dispersal, dormancy, germination and mucilage production upon imbibition (Arshad *et al.*, 2019; Baskin *et al.*, 2014; Lenser *et al.*, 2016; Lu *et al.*, 2015; Wang *et al.*, 2020; Yang *et al.*, 2015). These heteromorphic diaspore traits have been proposed to be an adaptive bet-hedging strategy to cope with spatiotemporally variable environments (Baskin *et al.*, 2014; Imbert, 2002), but very little is known about the underpinning mechanisms governing diaspore development into distinct morphs. A deep understanding of heteromorphism at the phenotypic level is crucial for molecular studies and is hampered in many heteromorphic systems by the high number of morphs, production of intermediate morphs and lack of a published genome sequence.

Here, we exploit the fruit and seed dimorphism in *Aethionema arabicum* (Figure 1), an annual member of the earliest diverging sister tribe (Aethionemeae) within the Brassicaceae (Lenser *et al.*, 2016; Mohammadin *et al.*, 2017), to investigate early morph-transitioning by advanced 3D imaging [synchrotron-based radiation X-ray tomographic microscopy (SRXTM)] and transcriptome analysis. Two distinct morphs of fruits and seeds are produced on the same individual infructescence (Figure 1a). DEH fruits release four to six non-deep dormant, mucilaginous (M^+) seeds. The surface of the dry mature M^+ seed coat is visible as an array of compressed, large circular-hexagonal cell outlines with thickened cell walls, representing mucilage-producing, conical papillae, which are irreversibly extruded upon seed imbibition (Figure 1b). In contrast, IND fruits each contain a single, pericarp-imposed deep dormant non-mucilaginous (M^-) seed (Figure 1b). No intermediate fruit or morphs are produced (Lenser *et al.*, 2016). While the multiple-seeded DEH fruits are predominantly produced on main flowering branches, single-seeded IND fruits in contrast are favoured on higher-order side branches (Lenser *et al.*, 2018). The strict dimorphism, together with available genome and transcriptome sequences (Fernandez-Pozo *et al.*, 2021; Nguyen *et al.*, 2019) (Wilhelmsson *et al.*, 2019), make *Ae. arabicum* an excellent model system for investigating the mechanisms of diaspore dimorphism.

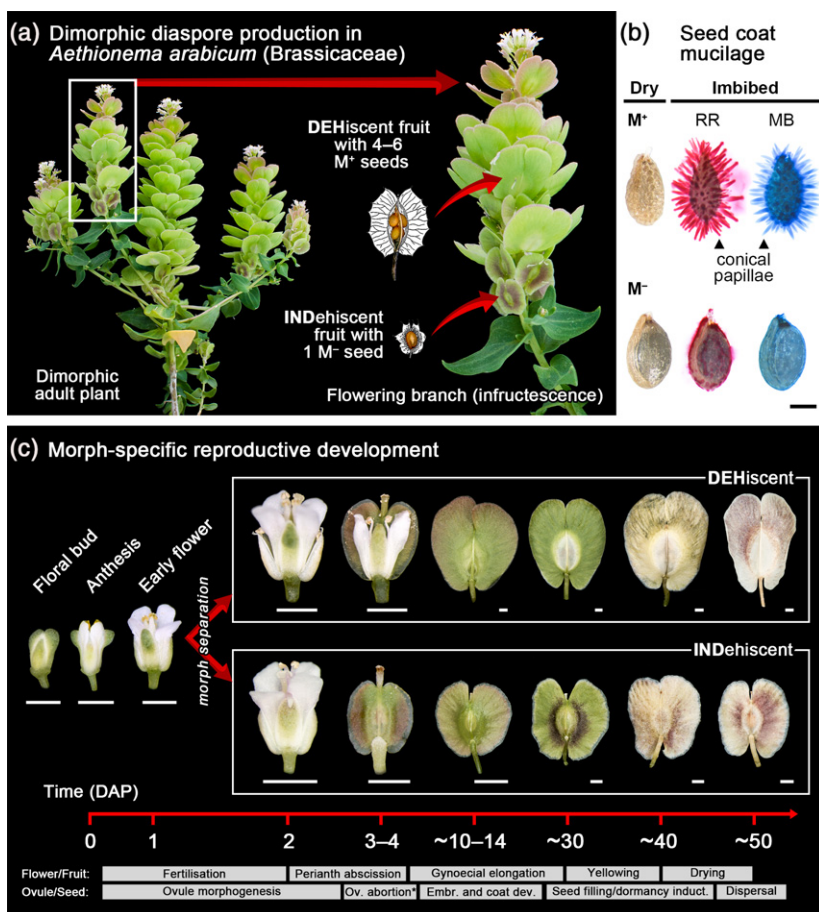


Figure 1. Fruit and seed dimorphism in *Aethionema arabicum* (Brassicaceae).

(a) Mature individual plant showing presence of two morphologically distinct fruit types on the same infructescence. Large, dehiscent (DEH) fruits contain four to six seed diaspores, which produce mucilage (M⁺) upon imbibition. Small, indehiscent (IND) fruits contain a single non-mucilaginous (M⁻) seed only. There are no intermediate fruit or seed morphs.

(b) Staining with ruthenium-red (RR) and methylene blue (MB) shows mature seeds from DEH fruits contain a pectin- and cellulose-rich, M⁺-forming epidermal cell layer that extrudes as conical papillae upon imbibition. In contrast, mature seeds manually excised from IND fruits possess a smooth, almost 'non-mucilaginous' outermost seed coat layer.

(c) Two fruit morphs have distinct patterns of reproductive development. Floral buds and flowers at anthesis (time at which self-pollination occurs) are phenotypically identical. Morph-specific differences become first evident 2 days after pollination (DAP), when fruit tissue growth extends beyond sepals in DEH fruits, while IND fruits remain concealed by outer floral organs. At 3–4 DAP, there is abscission of sepals and petals from both fruit morphs. Fruits elongate (4–30 DAP) through both cell expansion and cell division, before reaching their full length approximately 30 DAP, after which the fruit yellows (approximately 40 DAP) before drying. Scale bars = 1 mm.

RESULTS AND DISCUSSION

Co-ordinated time-course of *Aethionema arabicum* fruit and seed development reveals early initiation of morph-specific changes in seed coat differentiation

To establish key developmental events during the transition from flower bud to dimorphic fruit, a sequential account of the structural formation of reproductive organs in *Ae. arabicum* is provided (Figure 1c) by reference to the post-fertilization stages of *A. thaliana* gynoecium development (Ferrandiz *et al.*, 1999; Roeder and Yanofsky, 2006). In *Ae. arabicum*, fruit development follows a comparable pattern at initial stages from primordial bud formation to floral morphogenesis (Figure 1c). The lack of visible morph-specific external differences at the bud and early flower stage makes comparative analysis of *Ae. arabicum* morph differentiation difficult. To overcome the experimental problem that during the initiation of distinct morph differentiation to discriminate morphologically between the DEH and IND morphs may not yet be possible visually, we took advantage of the fact that fruit morphs are not distributed evenly throughout the plant (Lenser *et al.*, 2016, 2018). These earlier publications demonstrated that >95% of fruits

produced on second-order branches of undisturbed plants are IND morphs, and that 95% of fruits produced on the main branch of plants where the side branches are constantly removed are DEH morphs. This established experimental approach was used in our work for the imaging and the RNA-sequencing (RNA-seq) sampling. To verify the molecular results of the RNA-seq experiment, we used reverse transcription-quantitative polymerase chain reaction (RT-qPCR) with the same approach for the IND sampling, but for the DEH sampling we harvested from the undisturbed main branch across multiple plants. In this independent RT-qPCR experiment with independent biological RNA samples we combined this with expanding the time course to 3 and 10 days after pollination (DAP) at which the morphs are visibly distinct (Figure 1). Together this provided verification of the identified gene expression patterns in independent experiments and a detailed coverage of the early stages of morph separation.

Figure 1 and Figure S1 show that to the point of anthesis (0 DAP), morphologies of flowers that would later produce DEH and IND fruits appeared phenotypically identical. Analysis of pollen showed no difference between morphs (Figure S2), and aniline blue-stained pollen tubes show no

difference in growth (Lenser *et al.*, 2018). While petals and sepals readily abscised from the IND morph at 3–4 DAP, perianth withering in the DEH morph did not occur until 6 DAP, despite initiation of lateral fruit elongation (Figure 1c). Thus, floral development until very early stages of gynoecium expansion appears phenotypically monomorphic from the outside. Beyond this, fruits became clearly dimorphic in their development when pericarp tissue began expansion at 5 DAP. Comparison of fruit maturation patterns showed that onset of DEH silicle yellowing (37 DAP) was approximately 7 days earlier than in the IND fruit morph (43 DAP). This is consistent with earlier work comparing the transcriptomes of *Ae. arabicum* dry seeds, which indicated that M^+ seeds may desiccate earlier and mature faster compared with M^- seeds (Wilhelmsson *et al.*, 2019). Thus, fruit maturation into a dispersal-ready propagule also seemingly occurred at a faster rate for the DEH morph (Figure 1c). This time-course therefore allowed the identification of externally visible key events before, and soon after, phenotypic morph separation.

To explore the internal anatomy underlying the morph-specific phenotypic changes, we performed comparative SRXTM during the time-course of DEH and IND reproductive development. SRXTM is non-destructive and has been used successfully to reveal cryptic features and internal structures of modern and fossil flowers, fruits and seeds (Arshad *et al.*, 2020; Friis *et al.*, 2014; Smith *et al.*, 2009a). Reconstructed digital sections of *Ae. arabicum* obtained by SRXTM provided excellent cell and tissue details (Figure S1). Floral buds (0 DAP) exhibited a morphologically well-structured gynoecium and immature stamens. Ovules at anthesis (0 DAP) in both DEH (Figure S1f) and IND (Figure S1g) morphs exhibit differentiated internal structures of an identical nature. External morphologies of the bud (Figure S1a,d) and flower at 1 DAP (Figure S2e,h) were also consistently monomorphic in their anatomy. Within early immature fruits (approximately 7 DAP), clear external and internal differences between the two seed morphs were visible (Figure S1i–n): DEH fruits possessed four to six fertilized ovules (developing M^+ seeds), while IND fruits possessed only one (developing M^- seeds). Therefore, the comparative SRXTM imaging revealed that dimorphic fruits considerably differed in the early initiation of distinct seed coat development of their M^+ (within DEH fruits) and M^- (within IND fruits) seed morphs.

Dimorphic changes to the ovule wall and seed abortion are early post-fertilization processes

A temporal histological analysis of isolated gynoecia post-fertilization development indicated the more exact timing of changes to the wall of the ovules within developing fruits (Figure S3). The asymmetric growth of a single seed within IND fruits pushed the septum towards the side of the opposing seed chamber at 2–3 DAP, seemingly

resulting in the rupture of the septum and ‘fusion’ of the two locules (Figure S3f). The inner integument at 0–3 DAP consisted of multiple layers of parenchymatous cells during early seed development (Figure S3a–f), but later appeared as one or two layers of crushed palisade cells (Figure S3g–j). By 5 DAP, outer integuments had started differentiation into mucilage secretory cells in M^+ seeds only. Thus, the observed morphological changes associated with the transition of the integuments into the mature seed coat indicate that, at the same time as external differences between morphs become visible at 2–3 DAP, the developmental programme guiding seed coat mucilage development also becomes morph-specific. Consistent with earlier work demonstrating that seed abortion becomes visible in flowers at 2 DAP (Lenser *et al.*, 2018), we observed seed abortion in 2–3 DAP flowers of the IND programme (Figure S3f), demonstrating that it is a very early post-fertilization event. Together with the distinct morphological changes in seed coat development, this implies that the distinct molecular programmes driving *Ae. arabicum* seed and fruit dimorphism may be initiated very early in flowers upon fertilization.

Comparative RNA-seq analyses reveal transcriptomic differences during early morph-transitioning

For the transcriptome analysis, the described local separation of the fruit morph programmes allowed direct morph-specific comparisons during reproductive development by collecting bud (0 DAP), flower (1 DAP) and fruit (30 DAP) samples from the distinct branches representing the DEH fruit (M^+ seed) and the IND fruit (M^- seed) programmes, for which the RNA-seq analysis was conducted (Data S1). Replicate RNA-seq samples clustered tightly by organ (Figure 2a) and by morph (Figure 2b), as observed in a principal components analysis (PCA). The majority of the variability in the data was explained by PC1 (67.2%), while PC2 and PC3 explained 22.6% and 4.8% respectively, and clustering of samples for each stage separately demonstrating that early flower samples are much more distinct compared with bud samples (Figure 2c). An unsupervised hierarchical clustering approach based on Euclidean distance measures, also revealed the high similarity of bud samples from DEH and IND morphs (Figure 2d). However, while flower samples also clustered by morph, these samples were more similar in their transcriptional profile to bud samples than to fruit samples. These results suggest that the developmental trajectory of *Ae. arabicum* morphs is strongly evident from their transcriptional profile at the post-fertilization flower stage, but not at the bud stage of development.

Morph-specific analysis of differentially expressed genes (DEGs) detected significant differences at the three harvested stages (Figure 3). In total, 16 243 genes were found to be differentially expressed in IND versus DEH samples

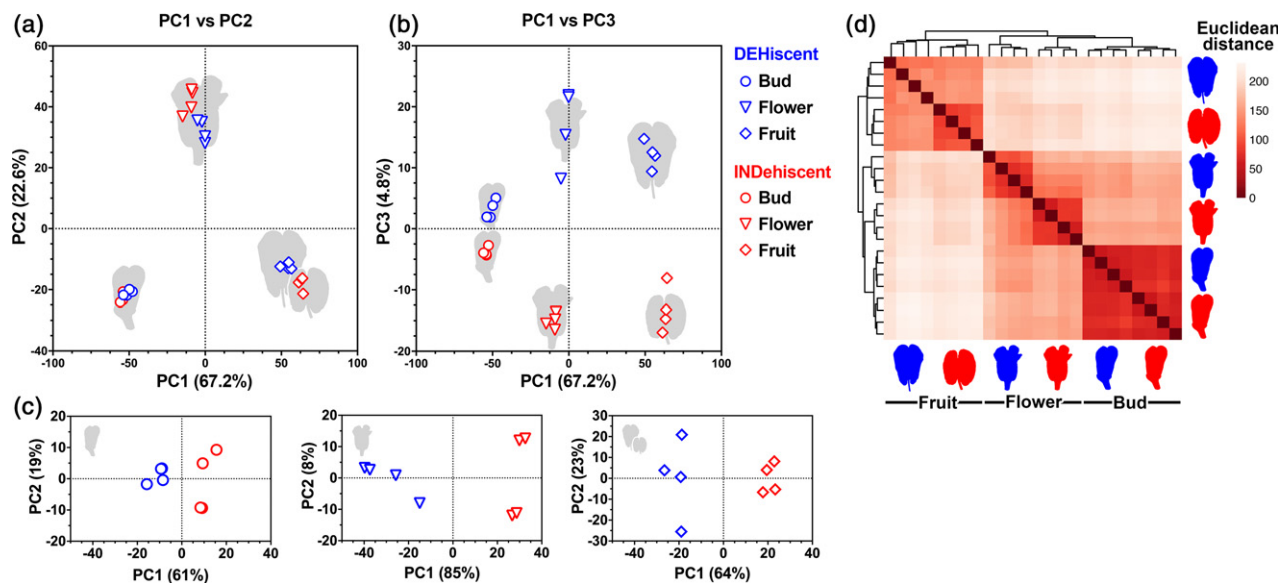


Figure 2. Comparative RNA-sequencing analysis of transcriptome dynamics during morph-specific reproductive development in *Aethionema arabicum*. (a,b) Unbiased principal components analysis (PCA) of morph-specific fruit development mRNA transcriptome data (Data S1). PCA plots are based on the top 500 genes by variance across all samples, using approximately homoscedastic Variance Stabilizing Transformed (VST) counts. Comparison of variable loadings on (a) PC1 versus PC2 and (b) PC1 versus PC3 reveal samples group in an organ-specific and morph-specific manner, respectively, with (c) clustering of biological replicates indicating the variation dominating the signal. (d) Unsupervised hierarchical clustering using VST count values, with heat map displaying a computed sample (Euclidean) distance matrix, reveals the high similarity of bud samples from dehiscent (DEH) and indehiscent (IND) morphs. Flower samples also cluster by morph, and are more similar in their transcriptional profile to bud samples than to fruit samples. At each stage of reproductive development, $n = 4$. Colours of bud, flower and fruit schematics indicate developmental morph (DEH, blue; IND, red).

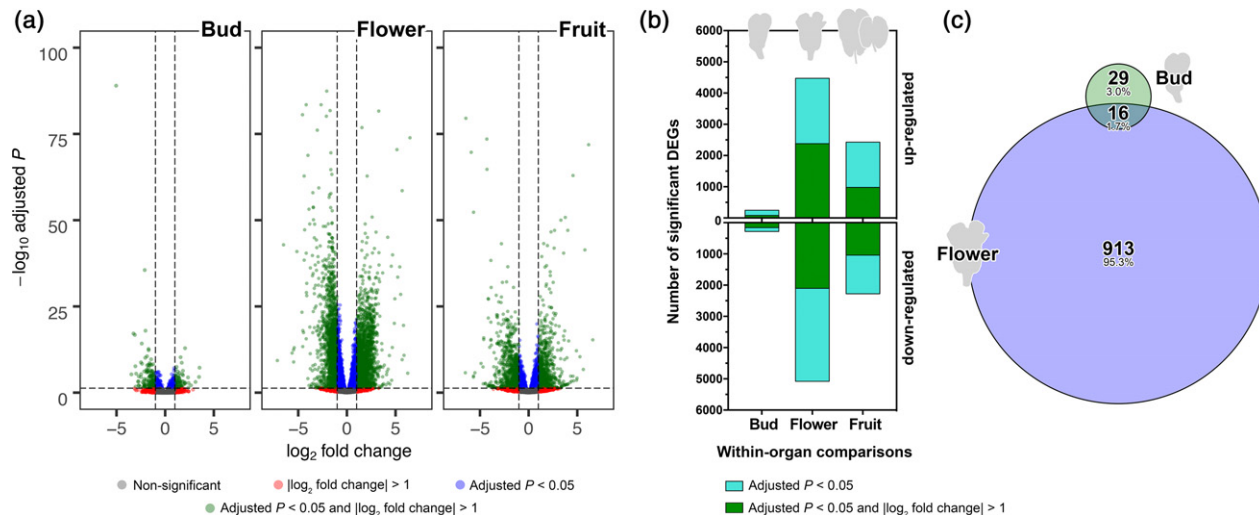


Figure 3. Differential expression analysis of morph-specific transcripts across reproductive development in *Aethionema arabicum*. (a) RNA-sequencing volcano plots of differential expression between *A. arabicum* morphs at bud [0 days after pollination (DAP)], flower (1 DAP) and immature fruit (30 DAP) developmental stages. Transcripts exhibiting a $|\log_2(\text{fold-change})| > 1$ and adjusted $P < 0.05$ were considered differentially expressed genes (DEGs). P values were generated with a negative binomial generalized linear model in DESeq2. (b) Summary of total (cyan) and $|\log_2(\text{fold-change})|$ significant (green) up- and downregulated transcripts based on morph-specific pairwise comparisons within each developmental stage. Shown are the transcriptional changes of indehiscent samples, with dehiscent samples set as the reference level. (c) Area-proportional Venn diagram depicting the numbers of shared DEGs across bud and flower stages.

(8012 upregulated and 8231 downregulated). The highest number of morph-specific DEGs were found at the flower (1 DAP) stage (in total, 4482 regulated at least 2-fold between DEH and IND, 2380 upregulated and 2102

downregulated; Figure 3). In contrast to this, fewer DEGs were identified at the bud (0 DAP, 240 DEGs) and immature fruit (30 DAP, 2022 DEGs) stages (Figure 3). Interestingly, $>8\%$ of the 4482 flower DEGs were TFs and other

master regulators interacting with TFs and RNA polymerase II to drive the morph-specific changes in fruit and seed (including ovule abortion in the IND programme) development observed (Figures 1 and 4; Figures S1 and S3). Analysis of gene ontology (GO) terms associated with up- and downregulated transcripts, showed significantly over- and under-represented GO terms of each class (molecular function and biological process; Data S2). Morph-specific GO comparison at the flower stage using Fisher's exact test, revealed for example that in the IND upregulated molecular function output list GO:0003700 (DNA-binding TF activity) was no. 3 and GO:0140110 (transcription regulator activity) was no. 5 with a false discovery rate corrected $P < 0.0001$ (Data S2). To investigate further the morph-specific role of mechanisms that control the transcription of genes we conducted motif enrichment analysis and compared it with the DEG results obtained for the different TF classes.

To analyse our *Ae. arabicum* datasets for motif enrichment we used the Analysis of Motif Enrichment tool of the MEME Suite (<http://alternate.meme-suite.org/tools/ame>) (McLeay and Bailey, 2010). Fisher's exact statistical test ($P < 0.01$, E value threshold 10) with comparison against the Arabidopsis DAP v1 database identified relatively enriched motifs (Data S3). Flower datasets delivered 331 enriched motifs, a higher number compared with the bud and fruit datasets (Data S3). The morph-specific enrichment in NAC, bZIP (basic leucine zipper), HD (homeodomain), AP2/EREBP (APETALA2/ethylene-responsive element binding proteins), C2H2 (C2H2 zinc finger), C2C2 (C2C2 zinc finger) and MYB-related promoter motifs indicate that these may be key targets of TFs in morph-specific processes; examples for identified bZIP, NAC, WRKY, HD and AP2/EREBP enriched motifs are presented in Figure S4. To analyse the expression patterns of TFs in the *Ae. arabicum* RNA-seq datasets we identified TFs using the Plant TF database PlnTFDB (Perez-Rodriguez *et al.*, 2010; Wilhelmsson *et al.*, 2017). This analysis identified 1552 *Ae. arabicum* TFs of which 366 were differentially expressed in the flower samples between the two morphs (Data S4; Figure 4b). Interestingly, 73.2% of these were upregulated in IND flower samples. This pattern was particularly evident for NAC, AP2/EREBP, HD, MYB, MADS, WRKY, C2H2, C2C2 and bZIP, but not for the bHLH and TCP class of TFs (Figure 4b). These expression patterns may indicate that they are key components of TF cascades initiating morph-specific programmes during ovule abortion, and other early seed and fruit developmental processes (Figure 4a).

Transcription regulators associated with post-fertilization ovule abortion within IND fruits

Given the systematic early abortion of seeds during IND fruit development (Figure 4; Figure S1), we examined RNA-seq data for candidate DEGs that may be involved

with this co-ordinated process preceding single M^- seed development. Forward genetic screens in *A. thaliana* identified genes involved in female gametogenesis and early embryo development, highlighting several maternal effect embryo arrest (MEE) mutants associated with defects in embryo sac development, fertilization and early embryogenesis (Pagnussat *et al.*, 2005). Of the nine identified MEE orthologues in *Ae. arabicum*, the *AearMEE14* and *AearMEE59* showed an increase in transcript abundances specifically within IND flower samples (Figure 5a). The approximately 9- and 2-fold increase, respectively, detected from normalized RNA-seq data was further investigated by RT-qPCR using independently grown samples at higher temporal resolution (Figure 5b). Interestingly, a time-dependent increase in expression was consistent for IND samples (developing a single M^- seed) in comparison with DEH samples (developing multiple M^+ seeds). Though IND transcript abundances showed considerable variation in the flower (1 DAP), expression levels showed a dramatic morph-specific difference at 3 DAP, where *AearMEE14* and *AearMEE59* expression correlates well with the timing of ovule abortion as observed by histology (Figure 4; Figure S3). It is known from work in *A. thaliana* that MEE14 encodes the central cell guidance-binding protein1 (CBP1), which acts as a mediator of transcription initiation in a complex with RNA polymerase II and TFs during fertilization (Li *et al.*, 2015). As in *Ae. arabicum* three ovules within the IND fruit are aborted at an early zygotic stage approximately 2–3 days post-fertilization, we speculate that *AearCBP1* through interaction with TFs may play a role in this highly morph-specific co-ordinated process. Interestingly, several of the *A. thaliana* MEE mutants have lesions in TF genes of the WRKY, MYB and TCP families (Pagnussat *et al.*, 2005). That we see an enrichment in WRKY- and MYB-, and TCP-related promoter motifs (Data S3, Figure S4) in *Ae. arabicum* IND flowers, in comparison with DEH flowers, may indicate that the corresponding TFs are key components in morph-specific processes during ovule abortion, and early seed and fruit development.

Almost all TFs associated with early morph-transitioning are upregulated in the IND programme

Consistent with the enrichment in WRKY-related promoter motifs (Figure S4), almost all of the 27 *Ae. arabicum* WRKY TF DEGs were upregulated in IND flower samples (Figure 4c). This upregulation at 1 DAP was 2–9-fold and two groups can be distinguished according to the expression patterns in immature fruits: the transcript abundances of 16 WRKY TF DEGs upregulated in IND flower samples (group A) were decreased to equal levels in fruit samples (Figure S5) suggesting that they play major roles in early morph-specific processes. An example for this is *AearWRKY28* (Figure 4c) for which the *A. thaliana* orthologue is known as a key component in ovule development

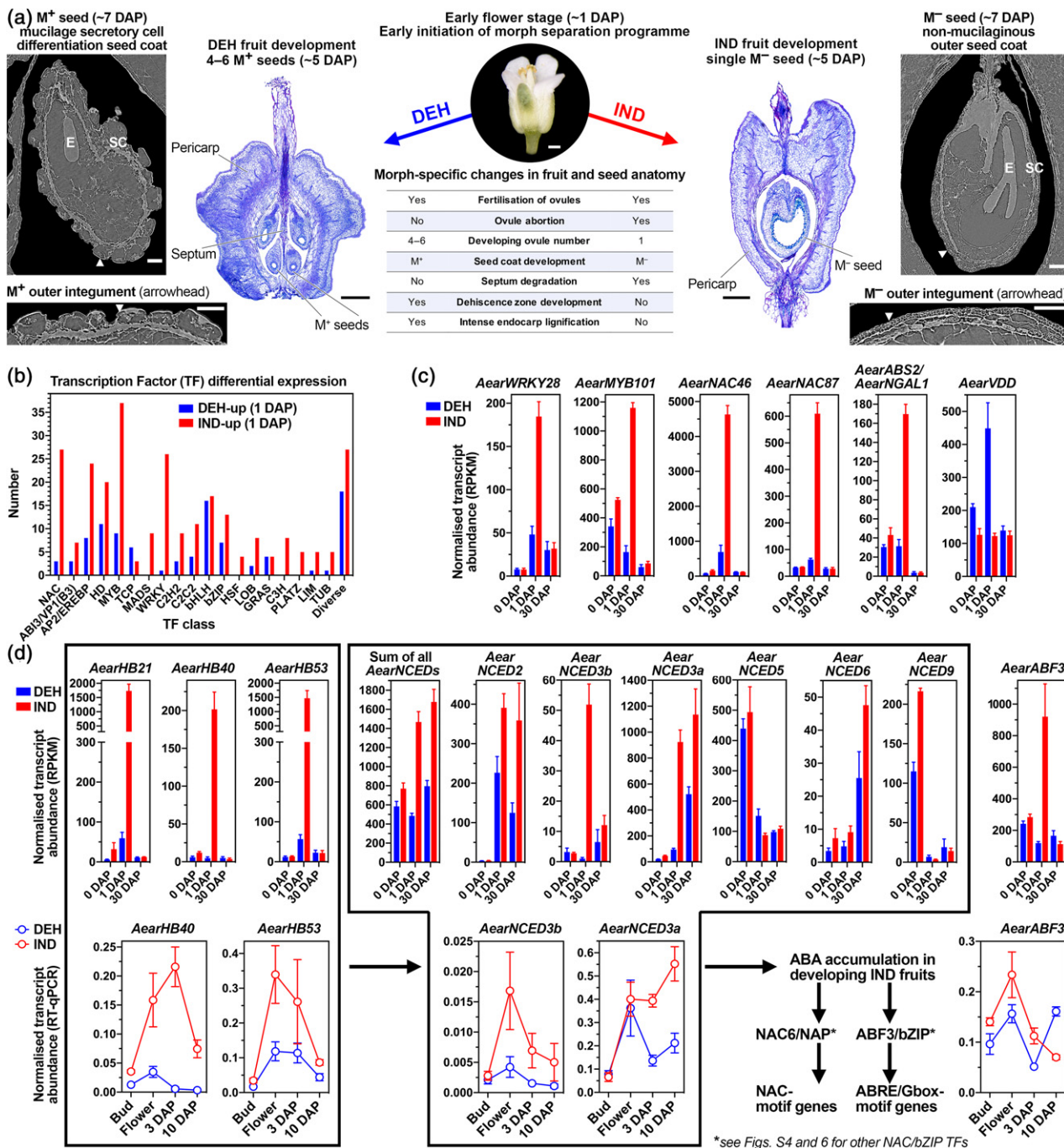


Figure 4. Differentially expressed transcription factor (TF) genes associated with morph-specific anatomical changes in the development of dehiscent (DEH) and indehiscent (IND) *Aethionema arabicum* fruits.

(a) Morph transition from a flower into a DEH or IND fruit is coupled with a multitude of gynoecial changes associated with the ovules, carpels, septum and pericarp tissue, as well as morph-specific early anatomical differences in early seed coat development. These changes lead to the development of non-deep dormant, mucilaginous (M⁺) seeds in DEH fruits, and the pericarp-imposed deep dormant, single non-mucilaginous (M⁻) seed in IND fruits. Shown are 6- μ m thick longitudinal sections of fruits at approximately 5 days after pollination (DAP), stained with toluidine blue. Scale bars = 300 μ m. Shown are synchrotron-based radiation X-ray tomographic microscopy (SRXTM) images of M⁺ (left) and M⁻ (right) seeds at approximately 7 DAP (see Figure S1 for detailed description of SRXTM). Scale bars = 75 μ m; E, embryo; SC, seed coat.

(b) Overview of differential expression (>2-fold; $P = 0.05$) of TFs; see Data S4 for details and expression values using the complete set of TFs of the PlnTFDB (Perez-Rodriguez et al., 2010; Wilhelmsson et al., 2017).

(c) Examples for TF differentially expressed genes in DEH and IND bud (0 DAP), flower (1 DAP) and fruit (30 DAP) samples. Mean \pm SE are presented. For gene names see main text.

(d) Transcript analysis of the BRC1/HD-ZIP/NCED cascade, which in *Arabidopsis thaliana* leads to abscisic acid (ABA) accumulation (Gonzalez-Grandio et al., 2017) and in *Ae. arabicum* differs between the morphs in that it is specifically upregulated in the IND programme.

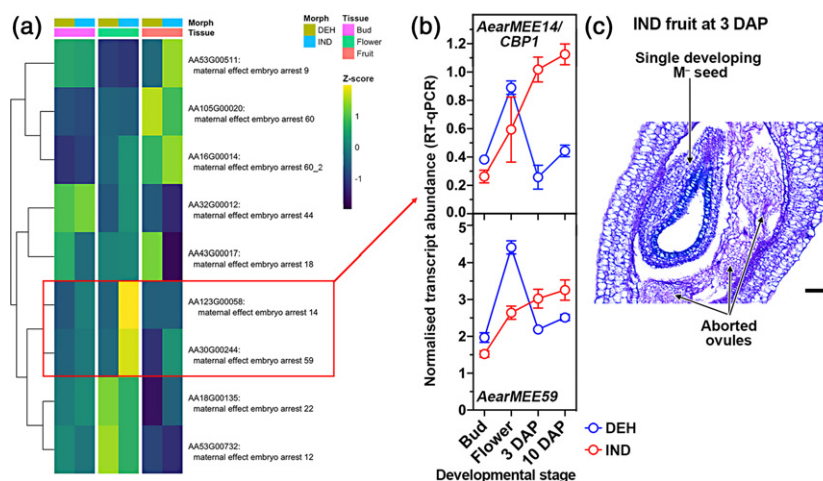


Figure 5. Ovule abortion in *Aethionema arabicum* indehiscent (IND) fruits.

(a) Clustered heatmap using the mean Z-score of the expression of nine identified *MATERNAL EFFECT EMBRYO ARREST* orthologues derived from RNA-sequencing data. Only the transcript abundance of the *Ae. arabicum* orthologue of *MEE14/CBP1* and *MEE59* correlates with the timing of controlled embryonic arrest (abortion) within indehiscent (IND) fruits approximately 2–3 days after pollination, as verified by reverse transcription–quantitative polymerase chain reaction (RT-qPCR) analysis (b) using independently grown biological samples. $n = 5$ (RT-qPCR) and $n = 4$ (RNA-sequencing); mean \pm SEM are presented. For gene names see main text.

(c) A toluidine-blue stained 6 μm thick section depicts the abortion of three ovules in IND gynoecia.

(Zhao *et al.*, 2018). The transcript abundances of the other 10 WRKY TF DEGs upregulated in IND flower samples (group B) were upregulated in DEH fruit samples, an example for this is *AearWRKY40* (Figure S5) for which the *A. thaliana* orthologue is known to be involved in responses to abscisic acid (ABA) (Ahmad *et al.*, 2019b). Interestingly, seed abortion in *Davidia involucreta* trees was associated with increased expression of most WRKY and MYB TFs (Li *et al.*, 2016). Likewise, 37 of the 46 *Ae. arabicum* MYB TF DEGs were upregulated in IND flower samples (Figure 4b). An example of these is *AearMYB101*, for which the *A. thaliana* orthologue is a key component in the fertilization process (Liang *et al.*, 2013), *AearMYB101* transcript abundances were 7-fold in IND versus DEH flower samples (Figure 4c). The NAC-domain TFs NAC046 and NAC087 are implicated in the developmentally controlled cell death in *A. thaliana* seedling root caps (Huysmans *et al.*, 2018). The observed 10- and 7-fold higher expression of *AearNAC46* and *AearNAC87*, respectively (Figure 4c); therefore, suggests they have roles in post-fertilization ovule abortion within IND fruits. Other *A. arabicum* NAC (Figures S4 and S5) and MYB TF DEGs in flower samples include NARS1/2 and MYB61 (Figure 6) known to be master regulators in mucilage deposition in *A. thaliana* outer seed coat development (Golz *et al.*, 2018; Kunieda *et al.*, 2008; Penfield *et al.*, 2001; Voiniciuc *et al.*, 2015; Western, 2012).

Members of the plant-specific B3-domain (ABI3/VP1; ABA INSENSITIVE3/VIVIPAROUS1) superfamily of TFs which are upregulated in *Ae. arabicum* IND flower samples include *AearABS2/AearNGAL1* (Figure 4c) and *AearVAL3* (Figure S5). Overexpression of ABNORMAL SHOOT2/

NGATHA-LIKE1 (*ABS2/NGAL1*) in *A. thaliana* leads to an early loss of flower petals (Shao *et al.*, 2012). In agreement with this, the 5-fold upregulation of *AearABS2/AearNGAL1* in *Ae. arabicum* IND flower samples (Figure 4c) is associated with an earlier loss of petals in IND fruits compared with DEH fruits (Figure 1c). Transcripts of *VP1/ABI3-LIKE3* (*VAL3*) and other B3-domain TFs are more strongly expressed in seedless grape cultivars (compared with seed-containing cultivars) and have been proposed to be involved in seed abortion and development seedlessness (Ahmad *et al.*, 2019a). In agreement with a possible role of *AearVAL3* in post-fertilization ovule abortion within IND fruits, its transcript abundances are approximately 2.5-fold higher in IND compared with DEH flower samples (Figure S5). An example for a B3-domain TF, which is stronger expressed in DEH (approximately 4-fold) compared with IND flower samples is *AearVDD* (Figure 4c). Silencing of the *VERDANDI* (*VDD*) gene leads to defects in fertilization and semi-sterility in *A. thaliana* (Matias-Hernandez *et al.*, 2010). These authors also showed that *VERDANDI* is the direct target of the MADS-domain TF *SEEDSTICK* (*STK*). A missense mutation in the grapevine orthologue of *A. thaliana* *STK* is associated with seed abortion leading to seedlessness in cultivated grapevine (Royo *et al.*, 2018). Transcript abundances of *AearSTK* are approximately 2.5-fold higher in IND compared with DEH flower samples (Figure 6). *SEEDSTICK* is a master regulator with many roles, including specifying ovule identity, fruit growth and septum fusion, seed coat development and mucilage production (Di Marzo *et al.*, 2020; Ezquer *et al.*, 2016; Golz *et al.*, 2018).

(a) Transcription Factors (TFs) - upper tier *Aethionema arabicum* seed coat epidermis (SCE) development

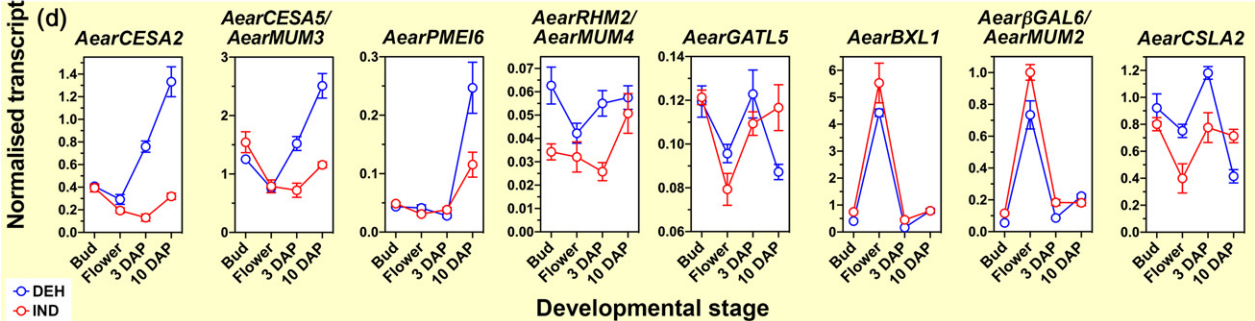
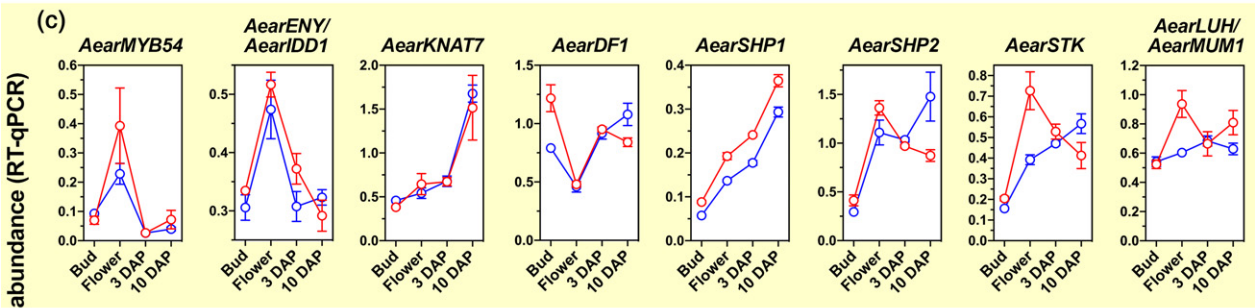
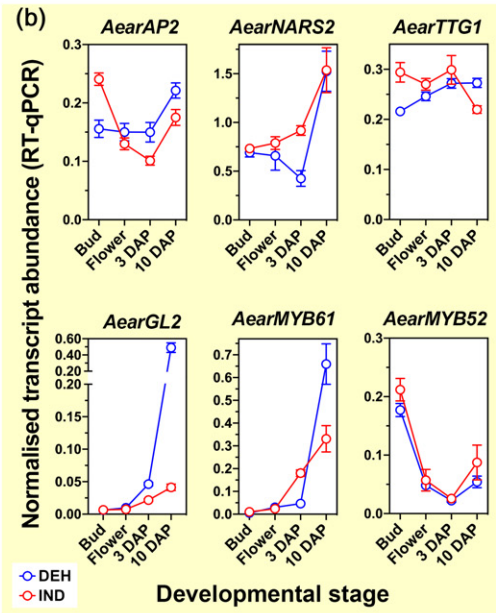
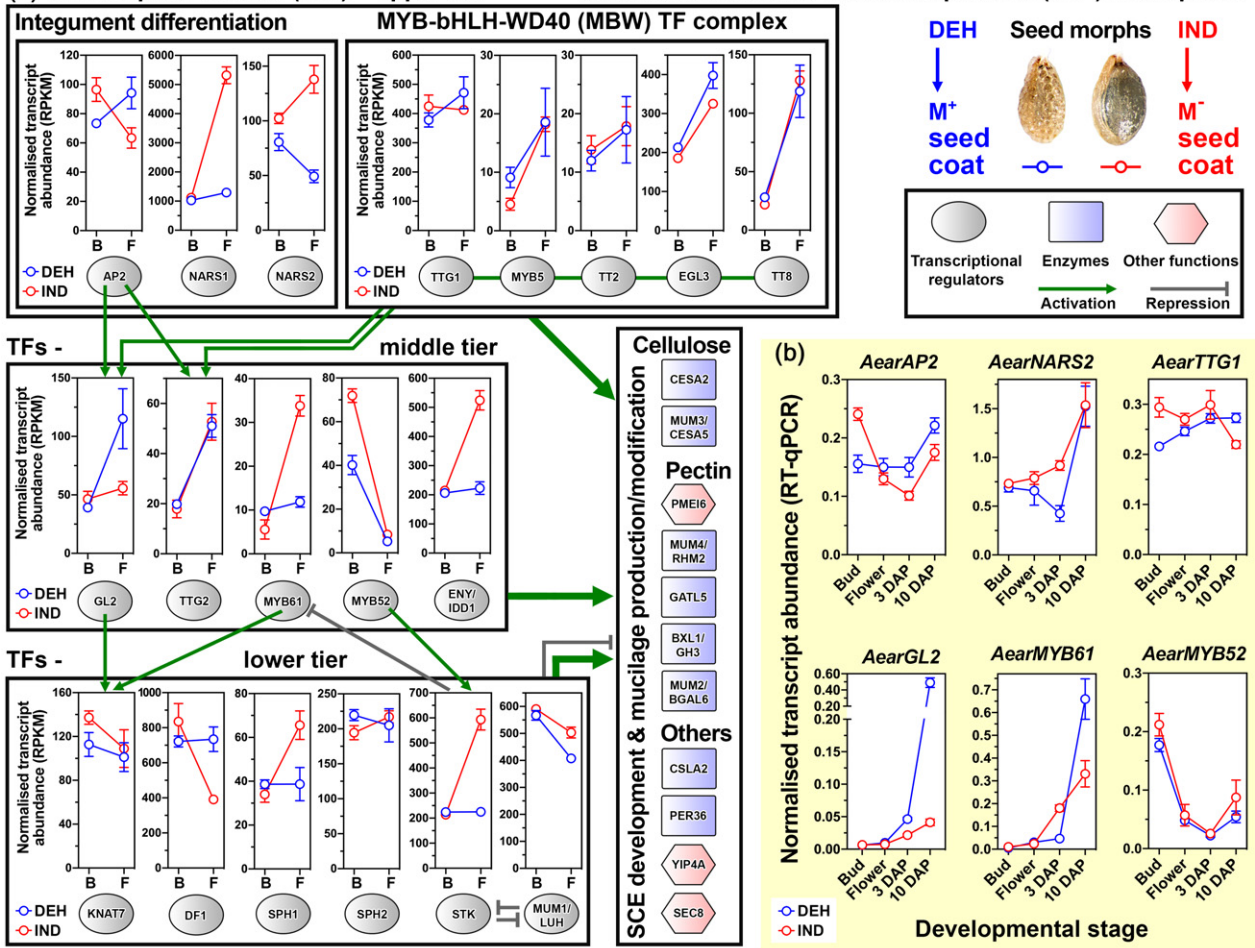


Figure 6. Comparative expression of transcriptional factor (TF) and cell-wall remodelling protein (CWRP) genes involved in *Aethionema arabicum* morph-specific early seed and fruit development and mucilage production.

(a) Normalized transcript abundances (RNA-sequencing) of *Ae. arabicum* dehiscent (DEH) and indehiscent (IND) bud [0 days after pollination (DAP)] and flower (1 DAP) samples for TF cascades known from *Arabidopsis thaliana* to control seed coat epidermis (SCE) differentiation and mucilage production (Golz *et al.*, 2018; Voiniciuc *et al.*, 2015).

(b,c) Comparative reverse transcription-quantitative polymerase chain reaction (RT-qPCR) of selected TF expression at 0–10 DAP in the DEH/M⁺ seed and the IND/M⁻ fruit/seed programmes. (d) Comparative RT-qPCR of representative CWRP marker genes for mucilage biosynthesis and modification. $n = 5$ (RT-qPCR) and $n = 4$ (RNA-sequencing); mean values \pm SEM are presented. For gene names see main text.

Homeodomain leucine zipper and ABA-related basic zipper TFs associated with early morph-specific seed and fruit development

Previous work with *Ae. arabicum* used RT-qPCR to reveal that the TEOSINTE BRANCHED1, CYCLOIDEA, PCF (TCP) TF *BRANCHED1* (*BRC1*), known to be a branching repressor, has a 7-fold increased transcript abundance in IND samples as compared with DEH samples at the early flower stage (Lenser *et al.*, 2018), which we confirmed here for *AearBRC1* expression in the RNA-seq data (Figure S5). Together with increased auxin and cytokinin contents at the early flower stage *BRC1* was proposed to be part of the molecular mechanisms for fruit morph decision (Lenser *et al.*, 2018). Interestingly, also the ABA contents increased 3-fold at the *Ae. arabicum* early flower stage in IND samples as compared with DEH samples. ABA accumulation and signalling is known as a hallmark of seed and bud dormancy (Finch-Savage and Leubner-Metzger, 2006; Gonzalez-Grandio *et al.*, 2017). Consistent with the deeper dormancy of *Ae. arabicum* M⁻ seeds and IND fruit diaspores as compared with the readily germinating M⁺ seeds, the increased ABA contents are maintained throughout the IND programme from early flowers to mature diaspores (Arshad *et al.*, 2019; Lenser *et al.*, 2016, 2018). ABA signalling inside *A. thaliana* buds is controlled by a TF cascade in which *BRC1* binds to and positively regulates the transcription of three homeodomain leucine zipper protein (HD-ZIP)-encoding genes *HOMEODOMAIN PROTEIN 21* (*HB21*), *HB40* and *HB53*, which leads to enhanced expression of the ABA biosynthesis gene *9-cis-EPOXYCAROTENOID DIOXIGENASE 3* (*NCED3*) and consequently to ABA accumulation (Gonzalez-Grandio *et al.*, 2017). We show here that the *BRC1*/HD-ZIP/NCED cascade is also evident in *Ae. arabicum* in the IND programme: *AearHB21*, *AearHB40*, *AearHB53* and *AearNCED* transcript abundances were higher specifically at 1 and 3 DAP in IND samples compared with DEH samples (Figure 4d). Phylogenetic analysis revealed that *Ae. arabicum* has two *AearNCED3* genes (Figure S6) and four of the six *AearNCED* were higher expressed in IND flower samples leading to 3-fold higher overall *AearNCED* transcript abundance at 1 DAP (Figure 4d). Seedlessness, ovule development and embryo abortion in grapes was also associated with enhanced expression of HD-ZIP TFs. Among the specifically upregulated TF genes in seedless grape cultivars was *VvHDZ09*,

which clusters very closely together with *A. thaliana* *HB21*, *HB40* and *HB53* in the phylogenetic analysis (Li *et al.*, 2017).

Gonzalez-Grandio *et al.* (2017) also demonstrated that among the downstream TFs induced by the *BRC1*/HD-ZIP/NCED cascade and the ABA accumulation are NAC TFs such as NAC-LIKE, ACTIVATED BY AP3/PT (NAP) and ABA-dependent bZIP TFs such as ABA RESPONSIVE ELEMENT (ABRE)-BINDING FACTOR3 (ABF3) and G-BOX BINDING FACTOR3 (GBF3). Consistent with a role of ABA-dependent TFs in early IND-morph development, transcripts of *AearABF3* (Figure 4d), *AearGBF3* and several other bZIP (Figure S5) TFs accumulate in IND flower samples. The same pattern is evident for *AearNAP* and several other NAC TFs (Figure S5). Together with HD-ZIP TFs, these ABA-dependent bZIP and NAC TFs are known to be master regulators in drought, heat, cold and salt stress responses as well as in secondary cell wall synthesis (Diao *et al.*, 2020; Hwang *et al.*, 2019; Taylor-Teeples *et al.*, 2015). As for the NAC and WRKY TFs, also most of the AP2-ERPBP and heat shock factor TF DEGs were upregulated in *Ae. arabicum* IND flower samples (Figure S5). The AP2-ERPBP are involved in regulating secondary cell wall synthesis (Taylor-Teeples *et al.*, 2015) and, as the heat shock factors, in abiotic stress responses (Guo *et al.*, 2016; Mizoi *et al.*, 2012). That 73% of the *Ae. arabicum* TF DEGs are upregulated in IND as compared with DEH flower samples is a characteristic for most or all of the TF families (Figure 4b). An important exception are the bHLH family TF DEGs for which examples in flower samples (Figure S5) include the IND-upregulated *DEFECTIVE REGION OF POLLEN1* (*DROP1*) known to be involved in fertilization (Zhang *et al.*, 2017), as well as the DEH-upregulated *INDEHISCENT* gene required for fruit valve opening (Mühlhausen *et al.*, 2013).

TF cascades and distinct downstream mucilage-related gene expression during morph-specific outer seed coat differentiation

Seed integuments showed considerable morph-specific differences already at approximately 7 DAP (Figure 4a), namely in the development and secretion of mucilage between the outer primary wall and the protoplast (in a ring around the area where starch granules are located within the cell) in developing M⁺ seeds (in DEH fruits). This secretion resulted in a ring-shaped mucilage pocket (Figure 4a; arrowhead). In contrast to this, the developing M⁻

seed coat (in IND fruits) comprised a more distinct, inner epidermal layer as well as several outer cell layers undergoing differentiation within the outer integument (Figure 4a). At approximately 40 DAP, the outermost epidermal layer formed large mucilage secretory cells in the case of mucilaginous seeds (M^+) from the DEH fruit morph (Figure S1p,q), but a thin outer epidermal layer lacking mucilage secretory cells in the single (M^-) seed (Figure S1r,s) of the IND fruit. Only several collapsed cell layers and an inner integument of relatively thick-walled cells remained in the developed and more differentiated M^- seed coat (Figure S1r). As both the SRXTM and histological approaches demonstrated key differences in patterns of mucilage synthesis and seed coat epidermis (SCE) development (Figure 4a; Figures S1 and S3), we hypothesized that the transcriptional network underpinning seed coat development in the M^- seed programme may be altered in a morph-specific manner as compared with the M^+ seed programme. The *Ae. arabicum* M^+ seed programme leads to a mucilaginous seed coat with polysaccharidic cell wall-like structures with large amounts of pectin combined with cellulose and hemicelluloses based on what is known from *A. thaliana* SCE development (Golz et al., 2018; Voiniciuc et al., 2015; Western, 2012).

Figure 6 depicts the three-tier SCE TF cascade known from *A. thaliana* and presents the comparative gene expression patterns from *Ae. arabicum* master regulators and exemplary downstream cell-wall remodelling genes. The RNA-seq data for the upper tier SCE TF (Figure 6a) revealed that the expression patterns of *NARS1/NAC2*, *NARS2/NAM* and the *APETALA2* (*AP2*) floral homeotic gene, differ between the two morphs. The NAC TF *AearNARS1/AearNARS2* was expressed roughly equally in buds ('B', 0 DAP), but were higher in IND flower samples (M^- seeds) as compared with DEH flower samples (M^+ seeds) ('F', 1 DAP). *NARS1/2* are master regulators of *A. thaliana* embryogenesis and the development of the outer integument. They are expressed in the outer seed coat, knock-out mutation and overexpression both lead to defects in outer seed coat development and mucilage deposition (Kunieda et al., 2008). The *Ae. arabicum* RNA-seq demonstrated that in contrast to *AearNARS1/2* and *AearAP2*, TFs of the MYB-bHLH-WD40 (MWB) complex (Golz et al., 2018; Viudes et al., 2020; Voiniciuc et al., 2015) did not show a morph-specific expression difference in flower samples (Figure 6a). Analysis of *AearAP2* and *AearNARS2* gene expression by RT-qPCR at 1, 3 and 10 DAP (Figure 6b) not only confirmed that the transcript abundances differ at the flower stage (1 DAP), but also during all the subsequent early stages of seed coat differentiation, particularly at 3 DAP. The upper-tier mucilage regulatory network (*AP2*, *NARS1/NAC2*, MWB complex) modulates the activity and expression of the middle-tier TFs (Figure 6a) to control outer seed coat differentiation

and mucilage production (Golz et al., 2018; Viudes et al., 2020; Voiniciuc et al., 2015).

AP2 and the MWB complex are required for the expression of the HD-ZIP TF *GLABRA2* (*GL2*) and the WRKY TF *TRANSPARENT TESTA GLABRA2* (*TTG2*), both of which act in the early stages of integument and epidermal cell differentiation (Golz et al., 2018; Viudes et al., 2020; Voiniciuc et al., 2015). Consistent with the finding that *Ae. arabicum* M^- seed coat programme is associated with altered seed coat development and reduced mucilage production (Figure 1; Figure S1), the RNA-seq data revealed a reduced induction of *AearGL2* expression IND flower samples (M^- seeds) as compared with DEH flower samples (M^+ seeds) (Figure 6a). RT-qPCR analysis (Figure 6b) demonstrated that this expression difference becomes even more pronounced at 3 and 10 DAP at which *AearGL2* is highly expressed in association with the M^+ seed coat programme leading to mucilage production and low in the M^- seed coat programme leading to non-mucilaginous seeds. Higher transcript abundance of the middle-tier MYB61 TF was evident in *Ae. arabicum* IND flower samples (Figure 6a). RT-qPCR verification showed for *AearMYB61* that this ratio shifts from being expressed higher in IND samples at 3 DAP to being expressed higher in DEH samples at 10 DAP (Figure 6b). In contrast to MYB61, the expression pattern for MYB52 did not differ (Figure 6a,b). Seeds of *A. thaliana* loss-of-function mutants in *AP2*, *GL2*, *TTG2*, *MYB61* and *MYB52* fail to release mucilage upon hydration due to a lack in mucilage secretory cell differentiation or defects in mucilage and columella production in the seed coat (Penfield et al., 2001; Western, 2012; Western et al., 2004). Several of these TFs are also involved in secondary cell wall formation, abiotic stress and ABA signalling. The middle-tier TFs, *GL2*, *MYB61* and *MYB52*, control the activity of lower-tier TFs, including the MADS-box TF *SEEDSTICK* (*STK*) and *SHATTERPROOF1/2* (*SHP1/2*) (Figure 6). *AearSTK* and *AearSHP1* gene expression is upregulated in IND samples (M^- seed programme) during the early stages, while it remains low in DEH samples (Figure 6). These TF are required for seed coat development and determine the mechanical properties of the seed coat (Ehlers et al., 2016; Ezquer et al., 2016; Golz et al., 2018). Seeds of *A. thaliana* *stk* mutants release only small amounts of mucilage and have altered cellulose-pectin matrixes of their cell walls.

The mucilage regulatory network of TF controls the expression of downstream genes involved in outer seed coat differentiation and mucilage production and modification (Golz et al., 2018; Viudes et al., 2020; Voiniciuc et al., 2015; Western, 2012). Prime targets include cellulose, hemicellulose and pectin biosynthesis, as well as pectin secretion and methylesterification. Two distinct and structured domains (layers) of extruded seed mucilage can be distinguished. In *A. thaliana* an inner adherent mucilage

layer is tightly associated with the seed and contains crystalline cellulose, hemicellulose, and as pectins rhamnogalacturonan I (RGI), homogalacturonan with differing degrees of methylesterification. In contrast to this, the outer water-soluble layer is almost exclusively composed of RGI pectin. Mucilage is modified and its extrusion is reduced or lacking in the *MUCILAGE-MODIFIED1-5* (*MUM1-5*) mutants. In this aspect they resemble *Ae. arabicum* M⁻ seeds, which exhibit significantly reduced mucilage extrusion (Figure 1b) and lack the conical papillae of M⁺ seeds (Lenser *et al.*, 2016). Ruthenium red (revealing the inner adherent mucilage layer) and methylene blue (highlighting columellae and cellulose rays) staining demonstrated that all components, including the cellulose rays for columella biosynthesis, are affected in M⁻ seeds (Figure 1b). In agreement with a reduction in cellulose biosynthesis, *CELLULOSE SYNTHASE (CESA)* gene expression was severely reduced during *Ae. arabicum* M⁻ seed coat development. The transcript abundances for *AearCESA2* and *AearCESEA5/AearMUM3* are 2–8-fold lower in 3–10 DAP M⁻ seeds as compared with M⁺ seeds (Figure 6d). The STK TF is upregulated in the *Ae. arabicum* M⁻ seed programme (Figure 6c), and is, consistent with the reduced *AearCESA2* expression, known in *A. thaliana* to inhibit *CESA2* expression directly (Ezquer *et al.*, 2016). Mucilage extrusion of *A. thaliana cesa5/mum3* seeds is reduced and lacks a structured adherent layer with reduced cellulose content (Sullivan *et al.*, 2011). These authors showed that *CESA5* is specifically expressed in the outer seed coat and the cellulose is required for anchoring the pectin components of mucilage to the seed.

PECTIN METHYLESTERASE (PME) and *PME-INHIBITOR (PMEI)* genes play crucial roles in seeds and mucilage properties with the *PMEI6* gene being specifically expressed in the outer seed coat to modify pectin properties (Ezquer *et al.*, 2016; Golz *et al.*, 2018; Saez-Aguayo *et al.*, 2013; Scheler *et al.*, 2015; Voiniciuc *et al.*, 2015). Mucilage release is delayed in *A. thaliana pmei6* mutants by increased methylesterification of the pectin homogalacturonan component. Several TFs including GL2, STK and MUM1/LUH are known to control *PMEI6* gene expression, with reduced expression of *PMEI6* in the *A. thaliana gl2* mutant. The transcript abundance for *AearPMEI6* is approximately 2.5-fold lower in 10 DAP M⁻ seeds as compared with M⁺ seeds (Figure 6d). Biosynthesis of the pectin RGI component requires the *RHAMNOSE BIOSYNTHESIS2 (RHM2/MUM4)* gene for which the *A. thaliana rhm2/mum4* mutant has severely reduced mucilage production (Usadel *et al.*, 2004; Western, 2012; Western *et al.*, 2004). Several TFs, including GL2 and MYB61, are known to control *RHM2/MUM4* gene expression and the production of RGI (Arsovski *et al.*, 2009; Penfield *et al.*, 2001). The transcript abundance for *AearRHM2/AearMUM4* is lower in 1–10 DAP M⁻ seeds as compared with M⁺ seeds (Figure 6d).

Consistent with a role of *AearGL2* in the reduced *AearRHM2/AearMUM4* and *AearPMEI6* expression, it is also expressed at reduced level in the M⁻ seeds programme (Figure 6a). GL2, MYB61, STK, MUM1/LUH and other TFs also control *GALACTURONOSYLTRANSFERASE-LIKE5 (GATL5)*, *β-GALACTOSIDASE6 (βGAL6/MUM2)* and other pectin-modifying genes (Golz *et al.*, 2018; Viudes *et al.*, 2020; Voiniciuc *et al.*, 2015; Western, 2012). Their differential expression may further contribute to the reduced production and modified properties of the *Ae. arabicum* M⁻ seed coat mucilage (Figure 1; Figures S1 and S6).

CELLULOSE SYNTHASE-LIKE A2 (CSLA2) is involved in the biosynthesis of galactomannan, a hemicellulosic polysaccharide in mucilage (Voiniciuc *et al.*, 2015). Mucilage of *A. thaliana csla2* mutant seeds is modified resulting in a more compact adherence layer and an altered spatial organization and reduced content of crystalline cellulose; and natural variation of *A. thaliana* seed mucilage was found to be associated with its differential expression (Voiniciuc *et al.*, 2016; Yu *et al.*, 2014). *AearCSLA2* expression differed between the M⁺ and M⁻ seed programme (Figure 6d) supporting the view that a complex morph-specific control by the *Ae. arabicum* transcriptional network affects all the mucilage polysaccharide components.

***Aethionema arabicum* as a dimorphic model for SCE development and differentiation in mucilage production**

The external surface of seed and fruit coats is extremely diverse, reflecting the multiple adaptations to environmental conditions. Upon imbibition of water, the diaspores of many species extrude mucilage from the outer seed coat (myxospermy) or fruit coat (myxocarpy) for which the adaptive value has attracted the attention of plant ecologists (Viudes *et al.*, 2020; Western, 2012; Yang *et al.*, 2012). The diaspore mucilage is typically composed of cellulose, pectin and hemicellulose polysaccharides, but 'true slimes' lacking cellulose are also known with flax seeds as an emerging model. Myxospermic Brassicaceae seeds, including *A. thaliana*, *L. sativum* and *Ae. arabicum* M⁺ seeds produce and extrude cellulosic mucilage in which crystalline cellulose provides structure and prevents mucilage from being washed away (Lenser *et al.*, 2016; Scheler *et al.*, 2015; Vaughan *et al.*, 1971; Western, 2012; Yang *et al.*, 2012). On the molecular level a set of *A. thaliana (mucilage-modified)* mutants has served to identify the mucilage TF network cascade and its downstream CWRP genes. The sequential evolution of myxodiaspory is evident from both the interspecies and intraspecies variability in these mucilage TFs and CWRPs expressed during outer seed coat development and mucilage secretory cell differentiation. Conserved TF cascades and CWRP genes were evident from a transcriptome analysis of *Artemisia spaerocephala* fruit coat mucilage biosynthesis, an example for a

myxocarpic species adapted to desert conditions (Han *et al.*, 2020; Yang *et al.*, 2011). We demonstrate here that *Ae. arabicum* provides an excellent dimorphic model system for SCE development in which the M⁺ seeds resemble the 'default' myxospermy pathway (as in the *A. thaliana* system) and the development of the non-mucilaginous M⁻ seed and IND fruit represent the non-myxospermic and non-myxocarpic pathways, respectively.

The advantage of the *Ae. arabicum* system is that the comparative molecular developmental pathways of myxospermy (M⁺ seeds) and non-myxospermy (IND fruits containing M⁻ seeds) can be studied on the same plant. For some TFs the reduced expression in the IND/M⁻ seed programme resembles the reduced mucilage production in *A. thaliana* mutants. The TF cascades combined with the SRXTM imaging also demonstrate that morph-specific developmental programmes are initiated very early post-fertilization. They were manifested by distinct expression patterns of master regulators and immediately followed by the expression of downstream genes leading to morph-specific developmental changes including the seed abortion in the IND/M⁻ programme and the distinct differentiation of mucilage production between the two morphs. The *Ae. arabicum* diaspora dimorphism is a blend of phenotypic plasticity and bet-hedging, two evolutionary modes of response to environmental variance (Arshad *et al.*, 2020; Arshad *et al.*, 2019; Bhattacharya *et al.*, 2019; Lenser *et al.*, 2016, 2018; Mohammadin *et al.*, 2017; Wilhelmsson *et al.*, 2019). A sequential evolution of the mucilage-associated TF and CWRP genes is evident in seed plants with natural variability within families, species and accessions, including in the Brassicaceae (Viudes *et al.*, 2020). Seed myxospermy is an advanced trait with an origin that may extend back to the Eocene, a geologic epoch with climatic variability and vegetation adaptation to long-term warming also evident from fossil fruits and seeds (Collinson *et al.*, 2012; Smith *et al.*, 2009b). SRXTM imaging of fossil (Friis *et al.*, 2019; Friis *et al.*, 2014; Manchester and Collinson, 2019; Smith *et al.*, 2009b) and modern (this work and Arshad *et al.*, 2020; Benedict *et al.*, 2016; Smith *et al.*, 2009b) flowers, seeds and fruits revealed internal structures that may have evolved as adaptations to climatic change and variable environments (Baskin and Baskin, 2014; Linkies *et al.*, 2010; Walck *et al.*, 2011).

EXPERIMENTAL PROCEDURES

Plant material and experimental growth conditions

Plants of *Aethionema arabicum* (L.) Andr. ex DC. were grown from accession no. ES1020 (Lenser *et al.*, 2018), in Levington compost with added horticultural grade sand (F₂ + S), under long-day conditions (16 h light/20°C and 8 h dark/18°C) in a greenhouse as described (Lenser *et al.*, 2018). The DAP was defined phenotypically as the time at which the flowers open (anthesis) and the four long stamens extend over the gynoecium.

SRXTM and classical microscopy of reproductive development

Five replicate buds, flowers, immature (approximately 7–10 DAP) fruits and mature (approximately 40 DAP) fruits were fixed in 3% glutaraldehyde plus 4% formaldehyde in 0.1 M piperazine-*N,N'*-bis(2-ethanesulfonic acid) (PIPES) buffer at pH 7.2. Samples were then rinsed with 0.1 M PIPES, and dehydrated in five changes of EtOH (30%, 50%, 70%, 95%, 100%). Critical point drying was performed on samples (Balzers CPD-030; Bal-Tec, Schalksmühle, Germany) that were then mounted on to 3 mm diameter brass pin stubs using two-component epoxy (Araldite[®]; Huntsman Advanced Materials GmbH, Basel, Switzerland) and imaged at the TOMographic Microscopy and Coherent rAdiology experimentTs (TOMCAT) beamline of the Swiss Light Source, Paul Scherrer Institute, Villigen, Switzerland (Stampanoni *et al.*, 2006). Data were acquired using a 10× objective and an sCMOS camera (PCO.edge; PCO, Kelheim, Germany), with an exposure time of 80 ms at 12 keV. Projections were post-processed and reconstructed using a Fourier-based algorithm (Marone and Stampanoni, 2012). Tomographic slice data derived from the scans were analysed using AVIZO[™] 9.5.0 (Thermo Scientific[™]; Visualization Science Group Inc., Burlington, MA, USA) for Windows 10 Pro 64-bit, and contrast adjusted in Adobe Photoshop Lightroom CC as described (Arshad *et al.*, 2020). Details of whole seed staining and microscopical analysis of seed coat differentiation are described in Supporting Information.

RNA-seq and molecular analyses of transcriptome data

Floral buds (0 DAP), flowers at anthesis (1 DAP) and immature fruits at their full length (30 DAP, before the onset of yellowing and drying) were harvested from second-order branches of plants that grew undisturbed (IND) or from the main branch of plants where side branches were constantly removed during development (DEH), as previously described by Lenser *et al.* (2018). Details of the extraction, quality control, processing and sequencing of four biological replicate RNA samples using 50-bp single-end mode on Illumina[®] HiSeq 2000 Analyzers are described in the Supporting Information. Data trimming, filtering, read mapping and feature counting, was as previously described (Wilhelmsson *et al.*, 2019); the details for this are also described in the Supporting Information. DEGs were identified using an adjusted *P*-value (false discovery rate) cut-off for optimizing the independent filtering set to 0.05 (Data S1). Details for the GO, promoter motif analyses (McLeay and Bailey, 2010) are described in the Supporting Information. Sequence data from *A. arabicum* are available in the CoGe database (<https://genomevolution.org/coge/>) under the following genome ID: v2.5, id33968.

Gene expression analysis via RT-qPCR

Floral buds (0 DAP), and flowers at 1, 3 and 10 DAP were harvested from second-order branches (IND) or from the main branch (DEH) of multiple undisturbed plants. Tissue was frozen in liquid nitrogen, and ground using a Precellys[®] 24 tissue homogenizer (Bertin Instruments, Montigny-le-Bretonneux, France). RNA was extracted using methods described for RNA-seq. The quantity and purity of RNA was determined using an Agilent 2100 Bioanalyzer with the RNA 6000 Nano Kit (Agilent Technologies, Santa Clara, CA, USA), using the 2100 Expert Software to calculate RNA Integrity Number (RIN) values. One microgram of DNase I-treated RNA was used for cDNA synthesis with random hexamer primers, using the Invitrogen[™] SuperScript[™] III First-Strand Synthesis System (ThermoFisher Scientific, Waltham, MA USA). RT-qPCR

reactions were performed in a CFX96 Touch™ Real-Time PCR Detection System (Bio-Rad, Watford, UK), using ABsolute qPCR SYBR Green Mix (ThermoFisher Scientific) and primer pairs listed in Table S1, with the following parameters: 95°C for 15 min, 40 cycles with 95°C for 15 sec, and 60°C for 30 sec, and 72°C for 30 sec, then 65°C for 31 sec. Melt-curve analysis verified the absence of primer-dimer artefacts and amplification of a single product from each qPCR assay. PCR efficiencies and C_q values were calculated using Real-time PCR Miner algorithm using raw fluorescence data as input (Graeber *et al.*, 2011). The geometric mean of *A. arabicum* orthologues of ADAPTIN FAMILY PROTEIN (*AearAFP*, AA44G00404), CALCINEURIN-LIKE METALLO-PHOSPHOESTERASE SUPERFAMILY PROTEIN (*AearCMSP*, AA10G00283), and the unknown protein AA19G00315 (*AearAA19G00315*) was used as reference for normalization. All RT-qPCR experiments were performed using five independent biological replicates. Statistical analysis was performed using GraphPad Prism (v.7.0a; San Diego, CA, USA), using a two-way ANOVA with a Šidák's *post-hoc* correction for multiple comparisons.

ACKNOWLEDGEMENTS

We thank Patricia Goggin and the Imaging and Microscopy Centre (University of Southampton, UK) for expert assistance with SEM and SRXTM sample preparation, and Sharon Gibbons (Earth Sciences, Royal Holloway University of London) for expert assistance with SEM. We acknowledge the excellent support by Zsuzsanna Merai, Sarhan Khalil, Ortrun Mittelsten Scheid (Gregor Mendel Institute of Molecular Biology, Vienna, Austria) and the Next Generation Sequencing unit at the Vienna BioCenter Core Facilities (VBCF) for collecting plant material and organizing the RNA sequencing. We also acknowledge the Paul Scherrer Institut, Villigen, Switzerland for provision of synchrotron radiation beamtime (Proposal ID: 20180809) at the TOMCAT beamline of the Swiss Light Source. We thank all members of the 'SeedAdapt' consortium project for fruitful discussions. This work was supported by a Natural Environment Research Council (NERC) Doctoral Training Grant to WA (NE/L002485/1), by the Deutsche Forschungsgemeinschaft (DFG) to GT (TH 417/10-1) and SAR (RE 1697/8-1), and by the Biotechnology and Biological Sciences Research Council (BBSRC) to GL-M and TS (BB/M00192X/1 and BB/M000583/1).

AUTHOR CONTRIBUTIONS

WA, TL, GT, TS, SAR and GL-M conceptualized and designed the research. WA, TL, JOC, TS and FM performed experiments. WA, TL, PKIW, JOC, TS, MEC, WS, FM, MP and GL-M analysed and interpreted data. WA and GL-M wrote the original manuscript draft. All authors commented on the draft and were thereby involved in shaping the manuscript. All authors reviewed and approved the final version of the manuscript.

CONFLICT OF INTEREST

The authors declare that they have no competing interests.

DATA AVAILABILITY STATEMENT

Single-ended Illumina raw reads from this study were uploaded to the NCBI Sequence Read Archive (SRA) and can be found under BioProject PRJNA639786 (<https://www.ncbi.nlm.nih.gov/bioproject/?term=PRJNA639786>). The mapping

data were uploaded to the Comparative genomics platform CoGe under 'Fruit development' experiments accompanying the v2.5 genome (<https://genomeevolution.org/coge/GenomeInfo.pl?gid=28950>).

SUPPORTING INFORMATION

Additional Supporting Information may be found in the online version of this article.

Figure S1. SRXTM imaging of *Aethionema arabicum* fruit morph development.

Figure S2. Scanning electron microscopy of *Ae. arabicum* pollen.

Figure S3. Morph-specific ovule anatomy of *Ae. arabicum*.

Figure S4. Analysis of motif enrichment in *Ae. arabicum* gene promoters.

Figure S5. Morph-specific differential expression of transcription factors.

Figure S6. Phylogenetic analysis of *Ae. arabicum* CCD genes.

Table S1. RT-qPCR primer sequences.

Data S1. Supporting data file with RNA-seq expression results.

Data S2. Supporting data file GO analysis.

Data S3. Supporting data file Enriched Motif Analysis.

Data S4. Supporting data file expression data for TF DEGs.

REFERENCES

- Ahmad, B., Zhang, S.L., Yao, J., Rahman, M.U., Hanif, M., Zhu, Y.X. *et al.* (2019a) Genomic organization of the B3-domain transcription factor family in grapevine (*Vitis vinifera* L.) and expression during seed development in seedless and seeded cultivars. *International Journal of Molecular Sciences*, **20**, 4553.
- Ahmad, R., Liu, Y., Wang, T.J., Meng, Q.X., Yin, H., Wang, X. *et al.* (2019b) GOLDEN2-LIKE transcription factors regulate WRKY40 expression in response to abscisic acid. *Plant Physiology*, **179**, 1844–1860.
- Arshad, W., Marone, F., Collinson, M.E., Leubner-Metzger, G. & Steinbrecher, T. (2020) Fracture of the dimorphic fruits of *Aethionema arabicum* (Brassicaceae). *Botany-Botanique*, **98**, 65–75.
- Arshad, W., Sperber, K., Steinbrecher, T., Nichols, B., Jansen, V.A.A., Leubner-Metzger, G. *et al.* (2019) Dispersal biophysics and adaptive significance of dimorphic diaspores in the annual *Aethionema arabicum* (Brassicaceae). *New Phytologist*, **221**, 1434–1446.
- Arsovski, A.A., Villota, M.M., Rowland, O., Subramaniam, R. & Western, T.L. (2009) MUM ENHANCERS are important for seed coat mucilage production and mucilage secretory cell differentiation in *Arabidopsis thaliana*. *Journal of Experimental Botany*, **60**, 2601–2612.
- Baskin, C.C. & Baskin, J.M. (2014) *Seeds - Ecology, biogeography, and evolution of dormancy and germination*. San Diego, London: Academic Press.
- Baskin, J.M., Lu, J.J., Baskin, C.C., Tan, D.Y. & Wang, L. (2014) Diaspore dispersal ability and degree of dormancy in heteromorphic species of cold deserts of northwest China: a review. *Perspectives in Plant Ecology, Evolution and Systematics*, **16**, 93–99.
- Benedict, J.C., Smith, S.Y., Specht, C.D., Collinson, M.E., Leong-Skornickova, J., Parkinson, D.Y. *et al.* (2016) Species diversity driven by morphological and ecological disparity: a case study of comparative seed morphology and anatomy across a large monocot order. *AoB Plants*, **8**, plw063.
- Bhattacharya, S., Sperber, K., Ozudogru, B., Leubner-Metzger, G. & Mummehoff, K. (2019) Naturally-primed life strategy plasticity of dimorphic *Aethionema arabicum* facilitates optimal habitat colonization. *Scientific Reports*, **9**, 16108.
- Collinson, M.E., Manchester, S.R. & Wilde, V. (2012) Fossil fruits and seeds of the Middle Eocene Messel biota, Germany. *Abhandlungen der Senckenberg Gesellschaft für Naturforschung*, **570**, 1–249.
- Di Marzo, M., Herrera-Ubaldo, H., Caporali, E., Novak, O., Strnad, M., Balanza, V. *et al.* (2020) SEEDSTICK controls *Arabidopsis* fruit size by regulating cytokinin levels and FRUITFULL. *Cell Reports*, **30**, 2846–2857.e3.

- Diao, P.F., Chen, C., Zhang, Y.Z., Meng, Q.W., Lv, W. & Ma, N.N. (2020) The role of NAC transcription factor in plant cold response. *Plant Signaling & Behavior*, **15**, 1785668.
- Ehlers, K., Bhide, A.S., Tekleyohans, D.G., Wittkop, B., Snowdon, R.J. & Becker, A. (2016) The MADS box genes ABS, SHP1, and SHP2 are essential for the coordination of cell divisions in ovule and seed coat development and for endosperm formation in *Arabidopsis thaliana*. *PLoS One*, **11**, e0165075.
- Ezquer, I., Mizzotti, C., Nguema-Ona, E., Gotte, M., Beauzamy, L., Viana, V.E. *et al.* (2016) The developmental regulator SEEDSTICK controls structural and mechanical properties of the Arabidopsis seed coat. *The Plant Cell*, **28**, 2478–2492.
- Fernandez-Pozo, N., Metz, T., Chandler, J.O., Gramzow, L., Merai, Z., Maumus, F. *et al.* (2021) *Aethionema arabicum* genome annotation using PacBio full-length transcripts provides a valuable resource for seed dormancy and Brassicaceae evolution research. *The Plant Journal*, **106**, 275–293.
- Ferrandiz, C., Pelaz, S. & Yanofsky, M.F. (1999) Control of carpel and fruit development in Arabidopsis. *Annual Review of Biochemistry*, **68**, 321–354.
- Finch-Savage, W.E. & Leubner-Metzger, G. (2006) Seed dormancy and the control of germination. *New Phytologist*, **171**, 501–523.
- Friis, E.M., Crane, P.R. & Pedersen, K.R. (2019) The endothelium in seeds of early angiosperms. *New Phytologist*, **224**, 1419–1424.
- Friis, E.M., Marone, F., Pedersen, K.R., Crane, P.R. & Stampanoni, M. (2014) Three-dimensional visualization of fossil flowers, fruits, seeds, and other plant remains using synchrotron radiation X-ray tomographic microscopy (SRXTM): new insights into Cretaceous plant diversity. *Journal of Paleontology*, **88**, 684–701.
- Golz, J.F., Allen, P.J., Li, S.F., Parish, R.W., Jayawardana, N.U., Bacic, A. *et al.* (2018) Layers of regulation—insights into the role of transcription factors controlling mucilage production in the Arabidopsis seed coat. *Plant Science*, **272**, 179–192.
- Gonzalez-Grandio, E., Pajoro, A., Franco-Zorrilla, J.M., Tarancon, C., Immink, R.G.H. & Cubas, P. (2017) Abscisic acid signaling is controlled by a BRANCHED1/HD-ZIP I cascade in Arabidopsis axillary buds. *Proceedings of the National Academy of Sciences of the United States of America*, **114**, E245–E254.
- Graeber, K., Linkies, A., Wood, A.T. & Leubner-Metzger, G. (2011) A guideline to family-wide comparative state-of-the-art quantitative RT-PCR analysis exemplified with a Brassicaceae cross-species seed germination case study. *The Plant Cell*, **23**, 2045–2063.
- Guo, M., Liu, J.H., Ma, X., Luo, D.X., Gong, Z.H. & Lu, M.H. (2016) The plant heat stress transcription factors (HSFs): structure, regulation, and function in response to abiotic stresses. *Frontiers in Plant Science*, **7**, 114.
- Guterman, Y. (2000) Environmental factors and survival strategies of annual plant species in the Negev Desert, Israel. *Plant Species Biology*, **15**, 113–125.
- Han, X.X., Zhang, L.J., Miao, X.M., Hu, X.W., Nan, S.Z. & Fu, H. (2020) Transcriptome analysis reveals the molecular mechanisms of mucilage biosynthesis during *Artemisia sphaerocephala* seed development. *Industrial Crops and Products*, **145**, 111991.
- Huysmans, M., Buono, R.A., Skorzinski, N., Radio, M.C., De Winter, F., Parizot, B. *et al.* (2018) NAC transcription factors ANAC087 and ANAC046 control distinct aspects of programmed cell death in the Arabidopsis columella and lateral root cap. *The Plant Cell*, **30**, 2197–2213.
- Hwang, K., Susila, H., Nasim, Z., Jung, J.Y. & Ahn, J.H. (2019) Arabidopsis ABF3 and ABF4 transcription factors act with the NF-YC complex to regulate SOC1 expression and mediate drought-accelerated flowering. *Molecular Plant*, **12**, 489–505.
- Imbert, E. (2002) Ecological consequences and ontogeny of seed heteromorphism. *Perspectives in Plant Ecology, Evolution and Systematics*, **5**, 13–36.
- Kunieda, T., Mitsuda, N., Ohme-Takagi, M., Takeda, S., Aida, M., Tasaka, M. *et al.* (2008) NAC family proteins NARS1/NAC2 and NARS2/NAM in the outer integument regulate embryogenesis in Arabidopsis. *The Plant Cell*, **20**, 2631–2642.
- Lenser, T., Graeber, K., Cevik, O.S., Adiguzel, N., Donmez, A.A., Grosche, C. *et al.* (2016) Developmental control and plasticity of fruit and seed dimorphism in *Aethionema arabicum*. *Plant Physiology*, **172**, 1691–1707.
- Lenser, T., Tarkowska, D., Novak, O., Wilhelmsson, P.K.I., Bennett, T., Rensing, S.A. *et al.* (2018) When the BRANCHED network bears fruit: how carpel dominance causes fruit dimorphism in *Aethionema*. *The Plant Journal*, **94**, 352–371.
- Li, H.J., Zhu, S.S., Zhang, M.X., Wang, T., Liang, L., Xue, Y. *et al.* (2015) Arabidopsis CBP1 is a novel regulator of transcription initiation in central cell-mediated pollen tube guidance. *The Plant Cell*, **27**, 2880–2893.
- Li, M., Dong, X.J., Peng, J.Q., Xu, W., Ren, R., Liu, J. *et al.* (2016) *De novo* transcriptome sequencing and gene expression analysis reveal potential mechanisms of seed abortion in dove tree (*Davidia involucreata* Baill.). *BMC Plant Biology*, **16**, 82.
- Li, Z.Q., Zhang, C., Guo, Y.R., Niu, W.L., Wang, Y. & Xu, Y. (2017) Evolution and expression analysis reveal the potential role of the HD-Zip gene family in regulation of embryo abortion in grapes (*Vitis vinifera* L.). *BMC Genomics*, **18**, 744.
- Liang, Y., Tan, Z.M., Zhu, L., Niu, Q.K., Zhou, J.J., Li, M. *et al.* (2013) MYB97, MYB101 and MYB120 function as male factors that control pollen tube-synergid interaction in *Arabidopsis thaliana* fertilization. *PLoS Genetics*, **9**, e1003933.
- Linkies, A., Gräber, K., Knight, C. & Leubner-Metzger, G. (2010) The evolution of seeds. *New Phytologist*, **186**, 817–831.
- Lu, J.J., Tan, D.Y., Baskin, J.M. & Baskin, C.C. (2015) Post-release fates of seeds in dehiscent and indehiscent siliques of the diaspore heteromorphic species *Diptychocarpus strictus* (Brassicaceae). *Perspectives in Plant Ecology, Evolution and Systematics*, **17**, 255–262.
- Manchester, S.R. & Collinson, M.E. (2019) Fruit morphology, anatomy and relationships of the type species of *Mastixcarpum* and *Eomastixia* (Cornales) from the late Eocene of Hordle, southern England. *Acta Palaeobotanica*, **59**, 51–67.
- Marone, F. & Stampanoni, M. (2012) Regridding reconstruction algorithm for real-time tomographic imaging. *Journal of Synchrotron Radiation*, **19**, 1029–1037.
- Matias-Hernandez, L., Battaglia, R., Galbiati, F., Rubes, M., Eichenberger, C., Grossniklaus, U. *et al.* (2010) VERDANDI is a direct target of the MADS domain ovule identity complex and affects embryo sac differentiation in Arabidopsis. *The Plant Cell*, **22**, 1702–1715.
- McLeay, R.C. & Bailey, T.L. (2010) Motif Enrichment Analysis: a unified framework and an evaluation on ChIP data. *BMC Bioinformatics*, **11**, 165.
- Mizoi, J., Shinozaki, K. & Yamaguchi-Shinozaki, K. (2012) AP2/ERF family transcription factors in plant abiotic stress responses. *Biochimica et Biophysica Acta*, **1819**, 86–96.
- Mohammadin, S., Peterse, K., van de Kerke, S.J., Chatrou, L.W., Donmez, A.A., Mummenhoff, K. *et al.* (2017) Anatolian origins and diversification of *Aethionema*, the sister lineage of the core Brassicaceae. *American Journal of Botany*, **104**, 1042–1054.
- Mühlhausen, A., Lenser, T., Mummenhoff, K. & Theissen, G. (2013) Evidence that an evolutionary transition from dehiscent to indehiscent fruits in *Lepidium* (Brassicaceae) was caused by a change in the control of valve margin identity genes. *The Plant Journal*, **73**, 824–835.
- Nguyen, T.P., Muhlich, C., Mohammadin, S., van den Bergh, E., Platts, A.E., Haas, F.B. *et al.* (2019) Genome improvement and genetic map construction for *Aethionema arabicum*, the first divergent branch in the Brassicaceae family. *G3: Genes, Genomes, Genetics*, **9**, 3521–3530.
- Pagnussat, G.C., Yu, H.J., Ngo, Q.A., Rajani, S., Mayalagu, S., Johnson, C.S. *et al.* (2005) Genetic and molecular identification of genes required for female gametophyte development and function in Arabidopsis. *Development*, **132**, 603–614.
- Penfield, S., Meissner, R.C., Shoue, D.A., Carpita, N.C. & Bevan, M.W. (2001) MYB61 is required for mucilage deposition and extrusion in the Arabidopsis seed coat. *The Plant Cell*, **13**, 2777–2791.
- Perez-Rodriguez, P., Riano-Pachon, D.M., Correa, L.G.G., Rensing, S.A., Kersten, B. & Mueller-Roeber, B. (2010) PlnTFDB: updated content and new features of the plant transcription factor database. *Nucleic Acids Research*, **38**, D822–D827.
- Roeder, A.H. & Yanofsky, M.F. (2006) Fruit development in Arabidopsis. *The Arabidopsis Book*, **4**, e0075.
- Royo, C., Torres-Perez, R., Mauri, N., Diestro, N., Cabezas, J.A., Marchal, C. *et al.* (2018) The major origin of seedless grapes is associated with a missense mutation in the MADS-box gene *VviAGL1*. *Plant Physiology*, **177**, 1234–1253.
- Saez-Aguayo, S., Ralet, M.C., Berger, A., Botran, L., Ropartz, D., Marion-Poll, A. *et al.* (2013) PECTIN METHYLESTERASE INHIBITOR6 promotes Arabidopsis mucilage release by limiting methylesterification of homogalacturonan in seed coat epidermal cells. *The Plant Cell*, **25**, 308–323.

- Scheler, C., Weitbrecht, K., Pearce, S.P., Hampstead, A., Buttner-Mainik, A., Lee, K. *et al.* (2015) Promotion of testa rupture during garden cress germination involves seed compartment-specific expression and activity of pectin methylsterases. *Plant Physiology*, **167**, 200–215.
- Shao, J.X., Liu, X.Y., Wang, R., Zhang, G.S. & Yu, F. (2012) The over-expression of an Arabidopsis B3 transcription factor, ABS2/NGAL1, leads to the loss of flower petals. *PLoS One*, **7**, e49861.
- Smith, S.Y., Collinson, M.E., Rudall, P.J., Simpson, D.A., Marone, F. & Stampanoni, M. (2009a) Virtual taphonomy using synchrotron tomographic microscopy reveals cryptic features and internal structure of modern and fossil plants. *Proceedings of the National Academy of Sciences of the United States of America*, **106**, 12013–12018.
- Smith, S.Y., Collinson, M.E., Simpson, D.A., Rudall, P.J., Marone, F. & Stampanoni, M. (2009b) Elucidating the affinities and habitat of ancient, widespread Cyperaceae: *Volkeria messelensis* gen. et sp. nov., a fossil mananioid sedge from the Eocene of Europe. *American Journal of Botany*, **96**, 1506–1518.
- Stampanoni, M., Groso, A., Isenegger, A., Mikuljan, G., Chen, Q., Bertrand, A. *et al.* (2006) Trends in synchrotron-based tomographic imaging: the SLS experience. *Developments in X-Ray Tomography V*, 6318. <https://doi.org/10.1117/12.679497>
- Sullivan, S., Ralet, M.C., Berger, A., Diatloff, E., Bischoff, V., Gonneau, M. *et al.* (2011) CESA5 is required for the synthesis of cellulose with a role in structuring the adherent mucilage of Arabidopsis seeds. *Plant Physiology*, **156**, 1725–1739.
- Taylor-Teeple, M., Lin, L., de Lucas, M., Turco, G., Toal, T.W., Gaudinier, A. *et al.* (2015) An Arabidopsis gene regulatory network for secondary cell wall synthesis. *Nature*, **517**, 571–575.
- Usadel, B., Kuschinsky, A.M., Rosso, M.G., Eckermann, N. & Pauly, M. (2004) RHM2 is involved in mucilage pectin synthesis and is required for the development of the seed coat in Arabidopsis. *Plant Physiology*, **134**, 286–295.
- Vaughan, J.G., Whitehouse, F.L.S. & Whitehouse, J.M. (1971) Seed structure and the taxonomy of the Cruciferae. *Botanical Journal of the Linnean Society*, **64**, 383–409.
- Viudes, S., Burlat, V. & Dunand, C. (2020) Seed mucilage evolution: diverse molecular mechanisms generate versatile ecological functions for particular environments. *Plant, Cell and Environment*, **43**, 2857–2870.
- Voiniciuc, C., Yang, B., Schmidt, M.H.W., Gunl, M. & Usadel, B. (2015) Starting to gel: how Arabidopsis seed coat epidermal cells produce specialized secondary cell walls. *International Journal of Molecular Sciences*, **16**, 3452–3473.
- Voiniciuc, C., Zimmermann, E., Schmidt, M.H.W., Gunl, M., Fu, L.B., North, H.M. *et al.* (2016) Extensive natural variation in Arabidopsis seed mucilage structure. *Frontiers in Plant Science*, **7**, 803.
- Walck, J.L., Hidayati, S.N., Dixon, K.W., Thompson, K. & Poschlod, P. (2011) Climate change and plant regeneration from seed. *Global Change Biology*, **17**, 2145–2161.
- Wang, Z.R., Baskin, J.M., Baskin, C.C., Yang, X.J., Liu, G.F. & Huang, Z.Y. (2020) Dynamics of the diaspore and germination stages of the life history of an annual diaspore-trimorphic species in a temperate salt desert. *Planta*, **251**, 87.
- Western, T.L. (2012) The sticky tale of seed coat mucilages: production, genetics, and role in seed germination and dispersal. *Seed Science Research*, **22**, 1–25.
- Western, T.L., Young, D.S., Dean, G.H., Tan, W.L., Samuels, A.L. & Haughn, G.W. (2004) MUCILAGE-MODIFIED4 encodes a putative pectin biosynthetic enzyme developmentally regulated by APETALA2, TRANSPARENT TESTA GLABRA1, and GLABRA2 in the Arabidopsis seed coat. *Plant Physiology*, **134**, 296–306.
- Wilhelmsson, P.K.I., Chandler, J.O., Fernandez-Pozo, N., Graeber, K., Ullrich, K.K., Arshad, W. *et al.* (2019) Usability of reference-free transcriptome assemblies for detection of differential expression: a case study on *Aethionema arabicum* dimorphic seeds. *BMC Genomics*, **20**, ARTN 95.
- Wilhelmsson, P.K.I., Muhlich, C., Ullrich, K.K. & Rensing, S.A. (2017) Comprehensive genome-wide classification reveals that many plant-specific transcription factors evolved in streptophyte algae. *Genome Biology and Evolution*, **9**, 3384–3397.
- Yang, F., Baskin, J.M., Baskin, C.C., Yang, X., Cao, D. & Huang, Z. (2015) Effects of germination time on seed morph ratio in a seed-dimorphic species and possible ecological significance. *Annals of Botany*, **115**, 137–145.
- Yang, X., Baskin, J.M., Baskin, C.C. & Huang, Z. (2012) More than just a coating: ecological importance, taxonomic occurrence and phylogenetic relationships of seed coat mucilage. *Perspectives in Plant Ecology, Evolution and Systematics*, **14**, 434–442.
- Yang, X., Zhang, W., Dong, M., Boubriak, I. & Huang, Z. (2011) The achene mucilage hydrated in desert dew assists seed cells in maintaining DNA integrity: adaptive strategy of desert plant *Artemisia sphaerocephala*. *PLoS One*, **6**, e24346.
- Yu, L., Shi, D.C., Li, J.L., Kong, Y.Z., Yu, Y.C., Chai, G.H. *et al.* (2014) CELLULOSE SYNTHASE-LIKE A2, a glucomannan synthase, is involved in maintaining adherent mucilage structure in Arabidopsis seed. *Plant Physiology*, **164**, 1842–1856.
- Zhang, J., Huang, Q.P., Zhong, S., Bleckmann, A., Huang, J.Y., Guo, X.Y. *et al.* (2017) Sperm cells are passive cargo of the pollen tube in plant fertilization. *Nature Plants*, **3**, 17079.
- Zhao, L.H., Cai, H.Y., Su, Z.X., Wang, L.L., Huang, X.Y., Zhang, M. *et al.* (2018) KLU suppresses megasporocyte cell fate through SWR1-mediated activation of WRKY28 expression in Arabidopsis. *Proceedings of the National Academy of Sciences of the United States of America*, **115**, E526–E535.